PFC/JA-84-22

Harmonic Emission from High-Power High-Frequency Gyrotrons

J.L. Byerly, B.G. Danly, K. E. Kreischer, R.J. Temkin
W.J. Mulligan, and P. Woskoboinikow
M.I.T. Plasma Fusion Center

June 1984

Abstract

The results of a study of second harmonic emission from a gyrotron designed for high power, high frequency operation at the fundamental of the cyclotron frequency are presented. Stable, very narrow bandwidth second harmonic cavity emission from 209 GHz to 302 GHz has been observed. An output power of 25 kW and efficiency of 6.5% in the $TE_{11,2,1}$ mode at 241 GHz is reported; this represents the highest power obtained to date from a high frequency (>100 GHz) harmonic gyrotron. These experiments have been carried out in a cavity for which the mode density is very high; the cavity diameter is approximately six free-space wavelengths for emission at the second harmonic. Mode competition between fundamental and second harmonic modes is discussed. It is also shown that, in general, gyrotrons designed for high power, low Q operation in overmoded cavities at the fundamental will also have high efficiencies and strong emission in second harmonic modes. Prospects for high frequency harmonic gyrotrons for plasma diagnostics and other applications are described.

1. Introduction

The gyrotron or electron cyclotron maser has proven to be one of the most promising new sources of high power, high frequency electromagnetic radiation. Its many applications include the RF heating of fusion plasmas (Alikaev et al. 1976; Gilgenbach et al. 1980), plasma diagnostics (Woskoboinikow et al. 1983), and radar.

We present here the results of a study of second harmonic emission from the M.I.T. gyrotron. This study is motivated by several considerations. Second harmonic emission can be both advantageous and disadvantageous to gyrotron design. The operation of a gyrotron at the second harmonic of the cyclotron frequency ($2\omega_c$) can produce radiation of a given frequency at a magnetic field half that required for operation at the fundamental. This allows the use of compact, less costly magnets. This study is also motivated by a concern for the possible deleterious effects of second harmonic oscillation in a gyrotron designed for operation at the fundamental. The existence of parasitic harmonics could cause damage to tube components or a decrease in the efficiency of operation at the fundamental.

During the past several years, impressive results have been obtained with gyrotrons designed for operation at harmonics of the cyclotron frequency. Zaytsev et al. (1974) have reported the generation of 7 kW at 154 GHz in pulsed operation and the generation of 2.4 kW at 157 GHz and 1.5 kW at 326 GHz in CW operation. Several harmonic experiments have also been carried out in the U.S. within the past decade (Jory 1977, Silverstein et al. 1982). An experiment in the People's Republic

of China has produced 30 kW at 37 GHz (Guo et al. 1981), and Thomson-CSF has reported the generation of 30 kW at 70 GHz by second harmonic operation (Boulanger et al. 1982). We report here the second harmonic generation of 25 kW at 241 GHz in pulsed operation; this represents the highest power obtained to date from a high frequency second harmonic gyrotron.

Because harmonic emission in high power, high frequency gyrotrons remains an important consideration for present and future gyrotron designs, a study of second harmonic emission in the M.I.T. 140 GHz gyrotron has been performed. This study includes both a theoretical analysis and experimental investigation. It represents, to our knowledge, the first study of harmonic emission in a large diameter ($D \sim 6\lambda$), highly overmoded cavity. This paper is organized as follows. In section 2, the linear and nonlinear theory for emission at the second harmonic ($2\omega_c$) in the M.I.T. gyrotron is presented. The gyrotron is described and the experimental results are presented in section 3. The results and their implications are discussed in section 4, and the conclusions of this second harmonic study are presented in section 5.

2. Theory

The initial phase of the second harmonic investigation involved the theoretical calculation of the frequency, starting current, and efficiency of all possible second harmonic modes in the 4-6 T magnetic field range. The lower limit of 4 T was chosen to ensure adequate beam quality; the upper limit was chosen to ensure that the fundamental mode frequencies remained well below the cutoff of the WR-3 band (220-325 GHz) waveguide used in the harmonic receiver. This range covers most of the previously observed (Temkin et al. 1982) fundamental modes.

The frequencies of the $2\omega_c$ modes in the 4-6 T range were calculated with a computer code (CAVRF) developed at the Naval Research Laboratory (Fliflet and Read 1981). This code numerically solves the wave equation for a weakly irregular gyrotron cavity to obtain the cavity eigenfrequency, the diffractive Q (Q_D) of the resonator, and the longitudinal profile of the RF electric field. The predicted frequency can then be compared with the measured value; the field profile and Q_D are required for the starting current and efficiency calculations.

The gyrotron cavity used for this study is the same as that for which previous experimental results at the fundamental have been reported (Temkin et al. 1982, Kreischer et al. 1984b). The cavity was designed for operation in the fundamental TE_{031} mode at a nominal frequency of 140 GHz. It has an input taper of 0.5° and an output taper of 4°. These tapers are sufficiently gradual that the CAVRF computer code should provide accurate values for Q_D and the second harmonic

frequency. In the 4-6 T magnetic field range, all TE_{mpq} modes with $q = 1$ and ν_{mp} in the range 14.8 to 22.0 were considered (ν_{mp} is the p^{th} zero of $J'_m(x)$). The higher order axial modes ($q > 1$) have been shown to have a substantially reduced diffractive Q ($Q_D \sim q^{-2}$) (Temkin 1981) and therefore were not considered. The diffractive Q for these second harmonic modes ranged from 3300 to 7700. The ohmic Q depends on the cavity mode and can be written as

$$Q_{OHM} \simeq \frac{R}{\delta}\left(1 - \frac{m^2}{\nu^2_{mp}}\right)$$

where R is the cavity radius and δ is the skin depth. Q_{OHM} ranges from a low of 6,000 for whispering gallery modes to approximately 20,000 for volume modes.

2.1 Linear Theory

The starting currents for the second harmonic modes in the 4-6 T range have been calculated from the linear theory developed by Kreischer and Temkin (1983). This linear theory assumes that the beam is weakly relativistic. Space charge effects and the interaction between the electrons and the RF magnetic field are neglected. These assumptions are justified for the beam parameters used in this experiment. The linear theory allows an arbitrary electron velocity distribution function; however, the startup current calculations presented here assume a single velocity, infinitely thin, annular electron beam. The effects of finite beam thickness on starting current are discussed in section 4.

Both the linear and nonlinear theories require the assumption of

a longitudinal field structure for the RF electric field. In both cases a Gaussian ($\exp(-(k_{\parallel}z)^2)$) was assumed. The full width of the Gaussian at the e^{-1} points is referred to as the effective length (L_{eff}) of the cavity and $k_{\parallel} = 2/L_{eff}$. The cold cavity longitudinal RF field profile is computed by the CAVRF computer code, and a Gaussian is fit to the exact profile to obtain L_{eff}.

The minimum starting current, frequency, and magnetic field for each $2\omega_c$ mode are tabulated in Table 1 for the experimental operating conditions of a beam voltage V_b = 64.3 kV and $v_{\perp}/v_{\parallel}$ =1.49. For each mode the starting current for both the co-rotating and counter-rotating TE modes has been calculated; only the smaller of the two starting currents is listed. With the exception of the whispering gallery type modes (TE_{m11}), all $2\omega_c$ modes have predicted starting currents of less than 6 A.

The starting current as a function of magnetic field for these $2\omega_c$ modes is shown in figure 1 and 2. Only a few of the starting current curves are labeled with the corresponding mode index; the others can be identified by reference to Table 1. Immediately apparent is the high density of $2\omega_c$ modes with low starting currents and their large degree of overlap. As is evident from Table 1 and figures 1 and 2, a large number of second harmonic modes should be observed experimentally.

2.2 Nonlinear Theory

In order to predict the efficiency of the $2\omega_c$ modes in Table 1,

a nonlinear theory is required. The nonlinear theory of a gyrotron with a Gaussian distribution for the longitudinal RF field was first developed by Nusinovich and Erm (1972). The slow time-scale, single particle equation of motion for an electron moving in a combined axial magnetic and RF electic field was integrated numerically. The results for both fundamental and second harmonic operation were presented in the form of isoefficiency contours in the I_o, μ plane. I_o is a normalized current defined by

$$I_o \equiv (0.24 \times 10^{-3})\, IQ_T \left(\pi \frac{\beta_\perp}{\beta_\parallel}\right)^{2(3-n)} \left(\frac{L_{eff}}{\lambda}\right)^{5-2n} \left(\frac{n^n}{2^n n!}\right)^2 \frac{J^2_{m\pm n}(k_\perp R_e)}{\left[\nu^2_{mp} - m^2\right] J^2_m(\nu_{mp})}$$

where R_e and R are the electron beam radius and cavity radius, $k_\perp = \nu_{mp}/R$, I is in amps, Q_T is the total Q, and n is the harmonic number. The normalized cavity length, μ, is defined by

$$\mu = \pi \frac{\beta^2_\perp}{\beta_\parallel} \frac{L_{eff}}{\lambda}$$

The particle orbits are integrated through the Gaussian longitudinal field distribution $f(\zeta) = \exp(-(2\zeta/\mu)^2)$ from $\zeta = -\sqrt{3}\mu/2$ to $+\sqrt{3}\mu/2$, where $\zeta = z\mu/L_{eff}$.

The theoretical efficiency of each of the $2\omega_c$ modes was calculated by a computer code which was developed at M.I.T. and based on the formulation of Nusinovich and Erm. For each second harmonic mode in Table 1, a Gaussian was fit to the calculated cold cavity longitudinal field profile in order to determine L_{eff} and μ; the perpendicular efficiency, $\eta_\perp$, was then calculated for the experimental conditions of V_b = 64.3 kV, I = 5A, and $v_\perp/v_\parallel$ = 1.49 at the cathode.

The calculated total efficiency for each $2\omega_c$ mode is shown in Table 2. This total efficiency, η, is related to $\eta_\perp$ by $\eta = \eta_\perp \eta_{el} \eta_Q$, where $\eta_{el} = \beta_\perp^2/\beta^2$ and $\eta_Q = Q_T/Q_D$. The values of the parameters μ, I_o, and Δ_{opt} are also shown in table 2. The magnetic field detuning, defined by $\Delta \equiv \frac{2}{\beta_\perp^2}(1 - \frac{2\omega_c}{\omega})$, for which maximum efficiency is achieved is denoted Δ_{opt}.

The efficiency of these $2\omega_c$ modes was also calculated for the integration limits $-\sqrt{3\mu}$ to $+\sqrt{3\mu}/2$. However, the resulting efficiences are approximately the same and are not tabulated here (Byerly 1984).

3. Experiment

The second harmonic experiment reported here was performed with the M.I.T. gyrotron which was designed for operation at the fundamental in the TE_{031} mode (Temkin et al. 1982) (Fig. 3). The electron beam is located at the second radial maximum of the TE_{031} mode. The electron gun produces a nonlaminar flow of electrons at the designed operating conditions of V_b = 65 kV and I = 5A (Felch et al. 1982). In addition to the main Bitter magnet, a gun coil is present at the electron gun to allow separate variation of the magnetic field at the cathode. This allows the magnetic compression to be maintained at the maximum possible value, resulting in the largest possible $v_\perp/v_\parallel$ at the cavity. There were four primary objectives for the experimental work: a magnetic field scan to detect second harmonic emission, frequency measurement for mode identification, starting current determination, and a calorimetric power level measurement for the stronger modes.

For the magnetic field scan, two receivers were positioned in the far field of the gyrotron output waveguide, as shown in Fig. 3. The second harmonic receiver consisted of a WR-3 band (220-325 GHz) horn, waveguide, attenuator and diode. The fundamental emission from the gyrotron was below the cutoff frequency of this receiver. The other receiver consisted of a WR-6 or D-band (110-170 GHz) horn, waveguide, attenuator and diode to detect the fundamental radiation. Because the D-band receiver responded to the second harmonic radiation, a two inch thick piece of plexiglass was placed in front of the fundamental receiver to absorb the $2\omega_c$ radiation while allowing most ω_c radiation to pass through to the diode. The magnetic field was then scanned from 4-6 T, and the attenuator settings required to maintain a constant

diode signal from both receivers was recorded. During the magnetic field scan, the gun coil magnets were periodically readjusted to maintain as high a compression ratio as possible without arcing.

The second harmonic modes were identified by a precise frequency measurement. The frequency measurement employed a harmonic mixing technique. A WR-3 band horn, waveguide, and attenuator were mounted on a WR-6 band harmonic mixer. The local oscillator was a YIG oscillator tunable from 12-16 GHz, with a frequency stability of ~ ±1 MHz. The RF pulse from the gyrotron was mixed with the local oscillator signal and the resulting intermediate frequency was dispersed with a surface acoustic wave filter and displayed on an oscilliscope. This diagnostic is described in detail elsewhere (Woskoboinikow et al. 1983b, Kreischer et al., 1984c).

A power measurement on several of the stronger modes was obtained by calorimetry. A calibration of the reflectivity versus frequency for two Scientech disk calorimeters was made with a dispersive Fourier transform spectrometer in the frequency range 100-400 GHz (Afsar 1982). The calorimeters have been previously modified to increase the absorption at millimeter wave frequencies (Kreischer et al. 1984b). In the frequency range of interest the absorption ranges from 65% to 90%. For the power measurement of a given $2\omega_c$ mode, the total power emitted from the gyrotron was measured. Then varying thicknesses of plexiglass absorber were used to attenuate the second harmonic radiation and the power measurement was repeated. By using an absorber with different absorption coefficients for the fundamental and $2\omega_c$ radiation (absorption scales roughly as frequency squared), the fraction of the total power resulting from $2\omega_c$

emission could be calculated. In practice, when the $2\omega_c$ radiation was strong enough to be measured with the calorimeter, greater than ~ 80 - 90% of the total output power was at the second harmonic. This typically occurred when the second harmonic mode had no nearby competing fundamental modes.

3.1 Experimental Results

The results of the magnetic field scan are shown in Fig. 4. The fundamental (unshaded) and second harmonic (shaded) zones of operation of the M.I.T. gyrotron are shown as a function of magnetic field. The ordinate represents the relative diode signal strength (log scale) of the ω_c and $2\omega_c$ modes. No quantitative comparison of the relative strengths of ω_c and $2\omega_c$ modes should be inferred from this figure, as the ω_c and $2\omega_c$ scans were performed with different diodes. Nor should a quantitative comparison between the amplitudes of two second harmonic zones of operation be inferred from this figure as the $2\omega_c$ diode responsivity over the observed range of frequencies was not known. Nonetheless, Fig. 4 serves to illustrate several important qualitative features of $2\omega_c$ operation and $\omega_c/2\omega_c$ mode competition. In general, strong $2\omega_c$ emission was observed in regions where no emission at the fundamental was present, while $2\omega_c$ emission was either suppressed completely or very weak in regions where strong emission at the fundamental was observed. This is discussed in more detail in section 4.

The harmonic mixer system was used to measure the frequencies of the observed second harmonic modes. This measurement allowed the identification of the mode. The measured frequencies are presented in Table 3, along with the mode index, the frequency that was predicted

from the CAVRF code, and the magnetic field at which the frequency determination was made. The indicies of the fundamental modes and the $2\omega_c$ modes which could be identified are also shown on Fig. 4.

The two strongest second harmonic modes observed were the $TE_{11,2,1}$ mode at 241.02 GHz and the $TE_{9,2,1}$ mode at 209.43 GHz. The power of these two modes was measured with the Scientech calorimeters. For the $TE_{11,2,1}$ mode, 25 ± 5 kW was obtained at 6A and 64.3kV. This represents the highest power ever obtained from second harmonic emission at a high frequency (> 100 GHz). This result corresponds to a total efficiency η ≈ 6.5%, as compared to a theoretical efficiency of 23%. The bandwidth of this 241.02 GHz emission was measured to be $\lesssim$ 5 MHz (FWHM), which is close to the transform limit, and the shot-to-shot frequency variations due to magnetic field fluctuations were ~ ±12 MHz. For the $TE_{9,2,1}$ mode, 15 kW was obtained at 6.6A and 64.3 kV at 209.43 GHz. This corresponds to a total efficiency of 3.5%. We estimate that the remaining $2\omega_c$ modes which were observed had powers in the 0.1 - 1.0 kW range.

The starting current was measured directly for the $TE_{11,2,1}$ mode. The beam current was gradually reduced at a constant cathode voltage while the WR-3 receiver and harmonic mixer system detected the continued presence of the mode. The magnetic field was adjusted to optimize the detuning as the current was reduced, and the minimum current for which the mode was present was measured. The starting current for the $TE_{11,2,1}$ mode was measured to be approximately 0.2A. This was lower than the predicted value of 1.13A.

Several factors could account for the discrepancies between the measured and theoretical values of the starting current and efficiency of the $TE_{11,2,1}$ mode. The ohmic Q may actually be much lower than its theoretical value. An ohmic Q roughly half the theoretical value would be comparable to the diffractive Q and thus reduce the total Q by a factor of two. This could reduce the efficiency considerably, although it would also raise the starting current. Beam velocity spread, the uncertainty over $v_\perp/v_\parallel$, or the possibility of a higher Q_D due to the improperly matched window (Kreischer et al. 1984c) could also contribute to these discrepancies.

Several important qualitative observations were made during the second harmonic experiments. For example, the simultaneous excitation of fundamental and second harmonic modes has been observed. Typical oscilliscope traces for the fundamental and second harmonic diode signals are shown in Fig. 5. The bottom trace is that of the RF pulse shape of the fundamental emission in the TE_{331} mode; the top trace is the RF pulse shape of the $2\omega_c$ emission. The magnetic field is at 5.98T. In all cases in which both ω_c and $2\omega_c$ emission were present simultaneously and the ω_c emission dominated the output, emission in the fundamental mode turned on first, with the second harmonic emission occurring after the ω_c emission had started.

Another qualitative observation was that the second harmonic emission appeared to have a strong dependence on the magnetic field at the cathode (as determined by the gun coil) and, hence, on the magnetic compression of the electron beam. In many cases, no $2\omega_c$ emission was observed at a particular setting of the main field unless the gun coil field was within a narrow range.

4. Discussion

These results demonstrate both the high power levels (25kW at 241 GHz) and high frequencies (302 GHz) that can be obtained from the second harmonic operation of a high frequency gyrotron. These experimental results also raise several important questions. Although eight $2\omega_c$ modes were observed, there are some 28 $2\omega_c$ modes with starting currents below 5A. This discrepancy is quite large.

An examination of Table 3 indicates a trend in the radial mode index p. With the exception of the $TE_{4,5,1}$ mode, each mode identified had radial mode numbers of p = 2 or p = 3. The linear theory predicted modes with $2 > p > 7$ to be above threshold and the modes with p = 4 to have the lowest starting currents. In order to attempt to explain the discrepancy between the observed $2\omega_c$ modes and predicted $2\omega_c$ modes, the effect of a finite electron beam thickness on the $2\omega_c$ starting currents was calculated. The beam-wave coupling factor, $G \equiv \frac{J^2_{m\pm n}\ (k_\perp R_e)}{\left[\nu^2_{mp} - m^2\right]\ J^2_m\ (\nu_{mp})}$, was replaced with an average over the finite beam width:

$$\overline{G} = \frac{\dfrac{1}{R_{e2} - R_{e1}} \displaystyle\int_{R_{e1}}^{R_{e2}} dR_e\ J^2_{m\pm n}\ (k_\perp Re)}{\left[\nu^2_{mp} - m^2\right]\ J^2_m\ (\nu_{mp})}$$

The electron beam was assumed to have a uniform spatial distribution between the maximum (R_{e2}) and minimum (R_{e1}) beam radii.

For the electron gun used in these experiments the beam thickness ($R_{e2} - R_{e1}$) has been determined by a computer simulation to be $3.5r_L$, where r_L is the Larmor radius (Felch et. al. 1982). Whereas the beam radius, R_e, was assumed to be 0.197cm for all the starting current calculations in Table 1, the beam radius varies in practice as the magnetic fields are varied. The starting current calculations have been repeated for the values of R_e and beam thickness appropriate to each $2\omega_c$ mode in Table 1. The recalculated starting currents, which are not tabulated here, differ by at most a factor of 2 and in most cases only by ± 30% from the values in Table 1 (Byerly, 1984). The incorporation of the finite beam thickness factor into the starting current calculations did not eliminate any of the $2\omega_c$ modes predicted to be present for the nominal operating current of 5A.

The only remaining plausible explanation for the paucity of $2\omega_c$ modes observed experimentally is that of mode competition. Both the linear theory (starting current calculations) and the nonlinear theory applied to second harmonic emission in section 2 assumed only one cavity mode present. As apparent from the diode scans (Fig. 4), for many magnetic field values, the simultaneous oscillation of two or more modes occurred. The existence of multimode oscillation at the fundamental of the cyclotron frequency is an important problem and has been discussed by several authors (Moiseev and Nusinovich 1974, Nusinovich 1981, Kreischer et. al. 1984a). Apparent in Fig. 4 are examples of $\omega_c/2\omega_c$ multimode oscillation, $2\omega_c/2\omega_c$ multimode oscillation as well as single mode oscillation at both ω_c and $2\omega_c$.

Both mode suppression and mode enhancement appear to be present. In most regions where there is strong fundamental emission present, the second harmonic emission is suppressed either partially or completely as with the $TE_{4,5,1}$, $TE_{13,2,1}$, $TE_{11,3,1}$, and $TE_{15,2,1}$ modes. In regions where strong ω_c emission is absent, emission at the second harmonic is much stronger, as with the $TE_{9,2,1}$, $TE_{7,3,1}$ and $TE_{11,2,1}$ modes. The simultaneous oscillation of three cavity modes was also observed in the case of one fundamental ($TE_{3,3,1}$) and two second harmonic ($TE_{11,3,1}$ and $TE_{15,2,1}$) modes. A quantitative theory of the competition between fundamental and second harmonic modes in a gyromonotron has been discussed by several authors (Zarnitsyna and Nusinovich 1977, Zapevalov et al. 1979, and Nusinovich 1981).

No third harmonic emission was detected from the gyrotron, in spite of the fact that five third harmonic modes were calculated to have starting currents of less than 5A and total efficiencies in the 5 - 10% range. Presumably, this absence of third harmonic emission was a result of the highly overmoded cavity used in this study; the high density of ω_c and $2\omega_c$ modes probably resulted in the mode suppression of the third harmonic modes.

The high efficiencies and low starting currents of the second harmonic modes observed in this experiment are not unique to the present experiment but rather are generally characteristic of high power gyrotrons designed for low Q operation at the fundamental. This may be demonstrated by a generalized analysis of the relative efficiency of ω_c and $2\omega_c$ mode emission from the same gyrotron cavity. The slow time scale

nonlinear theory with a Gaussian longitudinal field distribution (Nusinovich and Erm, 1972) and the contour plots of efficiency as a function of normalized current I_o and normalized cavity length μ for n^{th} harmonic operation provide a framework for this examination. We start by deriving a scaling law between I_o at the fundamental ($I_{o(n=1)}$) and I_o at the second harmonic ($I_{o(n=2)}$), and between μ at the fundamental ($\mu_{(n=1)}$) and second harmonic ($\mu_{(n=2)}$). Then the region in the I_o-μ plane corresponding to high efficiency, low Q gyrotron designs at the fundamental can be mapped to a region in the I_o-μ plane for second harmonic emission. This scaling is kept as mode independent and general as possible.

The relationship between μ at the fundamental and second harmonic can be shown to be

$$\mu_{(n=2)} \approx 2\mu_{(n=1)}$$

where we have neglected minor differences between effective cavity lengths (or $k_\parallel$). Computer simulations indicate that, for a given cavity design, L_{eff} is virtually the same for all modes excited in the cavity. To determine the scaling law for I_o, consider the ratio

$$\frac{I_{o(n=2)}}{I_{o(n=1)}} \approx \frac{2}{\pi^2}\left(\frac{\beta_\parallel}{\beta_\perp}\right)^2\left(\frac{\lambda}{L_{eff}}\right)^2_{(n=1)}\frac{Q_{(n=2)}}{Q_{(n=1)}}\frac{G_{(n=2)}}{G_{(n=1)}}$$

where G is the coupling factor defined previously.

At this point an estimate for the ratios of Q and G between the fundamental and second harmonic is required. A scaling of the Q can be

obtained by assuming the beam placement allows neglect of the whispering gallery modes; then $Q \sim Q_D$ and

$$Q_D = 4\pi \left(\frac{L_{eff}}{\lambda} \right)^2 \frac{1}{1 - |R_1 R_2|}$$

where R_1 and R_2 are the reflection coefficients for the ends of the cavity. Disregarding the slight difference of R_1 and R_2 for the ω_c and $2\omega_c$ modes, $Q_{(n=2)} \approx 4Q_{(n=1)}$.

The G factor is clearly mode specific. However, by assuming that the beam will be in a near optimum location to excite the second harmonic mode, we may assume that

$$\frac{J^2_{m\pm n}\,(k_\perp R_e)}{J^2_m\,(\nu_{mp})} \approx 1$$

for both the n=1 and n=2 modes. This reduces the G factor scaling to

$$\frac{G_{(n=2)}}{G_{(n=1)}} \approx \frac{\nu^2_{mp(n=1)} - m^2_{(n=1)}}{\nu^2_{mp(n=2)} - m^2_{(n=2)}}$$

The whispering gallery modes have already been disregarded; the neglect of other extreme surface modes allows the generalization $\nu^2_{mp} >> m^2$, with the resulting simplification.

$$\frac{G_{(n=2)}}{G_{(n=1)}} \approx \frac{\nu^2_{mp(n=1)}}{\nu^2_{mp(n=2)}} \approx \frac{1}{4}$$

This scaling factor was checked against actual G value ratios computed using the wall and beam radius values of the $TE_{0,3,1}$ cavity. Modes were chosen such that $\nu_{mp(n=2)} \approx 2\nu_{mp(n=1)}$; the resulting range

of $G_{(n=2)}/G_{(n=1)}$ is 0.12 to 0.46. Consequently this general scaling is accurate to within a factor of two under the mode restriction and beam placement assumptions. The final expression for $I_{o(n=2)}$ in terms of I_o at the fundamental can now be derived:

$$I_{o(n=2)} \approx \frac{2\beta_\perp^2}{\mu^2_{(n=1)}} \quad I_{o(n=1)}$$

This expression is not useful in consideration of specific modes, but provides an estimate of $I_{o(n=2)}$ and, consequently, the second harmonic efficiency for a particular range of I_o and μ at the fundamental.

Application of this scaling to the isoefficiency contour plots of Nusinovich and Erm (1972, Gaponov et. al. 1975) allows an estimation of $2\omega_c$ efficiencies for the high efficiency ($0.4 \leq \eta_\perp \leq 0.7$) zone of operation at the fundamental. The second harmonic perpendicular efficiencies predicted by this scaling are on the order of $0.2 \leq \eta_\perp \leq 0.4$, even including the rather large error bars. High frequency gyrotron devices operating at megawatt power levels at the fundamental are very likely to operate at high efficiency and low Q in highly overmoded cavities. These conditions could result in many second harmonic modes capable of high efficiency oscillation. Thus it is imperative that the possibility of second harmonic emission be considered in future designs of megawatt gyrotrons.

Of course, a full treatment of the effect of $2\omega_c$ emission on operation at the fundamental can only be obtained from a multimode treatment. Nevertheless, the high efficiencies for $2\omega_c$ emission in high power, low Q gyrotrons designed for operation at the fundamental require the consideration of harmonic emission in future gyrotrons.

5. Conclusions

We have presented a study of second harmonic emission in a high frequency, high power gyrotron designed for operation at the fundamental of the cyclotron frequency. Second harmonic emission has been observed at frequencies as high as 302 GHz and in eight identified modes. A record power level for $2\omega_c$ operation at high frequency has been obtained: 25 kW at 241 GHz in the $TE_{11,2,1}$ mode. Several qualitative observations have been made. Second harmonic emission appears strongest in magnetic field regions between fundamental modes. Second harmonic emission is also observed in regions of strong fundamental emission, but it is weak.

Several examples of multimode oscillation have been observed, including the simultaneous oscillation of two second harmonic modes. The multimode oscillation of two second harmonic modes and one mode at the fundamental has also been observed. For future megawatt and multimegawatt gyrotrons, mode competition from harmonic emission is a potential danger which must be considered.

The results of this survey of second harmonic emission indicate that the second harmonic generation of high power at high frequency is feasible. For example, the generation of high power radiation in the submillimeter band by harmonic emission appears practical although competition from modes at the fundamental must be avoided. This may be possible by a proper choice of oscillation mode, electron beam radius, cavity Q and other factors. Such high frequency gyrotrons operating CW or for long pulses could find application in plasma diagnostics or communications.

For these long pulse applications, operation at the second harmonic in superconducting solenoids appears more promising than the alternative of operation at the fundamental in pulsed solenoids (Luchinin et al. 1983).

Acknowledgements

We wish to thank D.R. Cohn for his encouragement and support throughout this work. We are grateful to the Francis Bitter National Magnet Laboratory and the National Science Foundation for the use of the high field Bitter magnet. This research was conducted under U.S.D.O.E. Contract DE-AC02-78ET-51013.

References

Afsar, M.N., 1982, Precision millimeter-wave complex dielectric permittivity measurements of low loss materials: One part in 10^5 measurement of the refractive index. NBS Conf. precision electromagnetic measurements Dig., IEEE Cat. 82CH1737-6.

Alikaev, V.V., Bobrovskii, G.A., Poznyak, V.I., Razumova, K.A., Sannikov, V.V., Sokolov, Yu.A., and Shmarin, A.A., 1976, ECR plasma heating in the TM-3 tokamak in magnetic fields up to 25kOe. Sov. J. Plasma Phys. 2, 212.

Boulanger, P., Charbit, P., Faillon, G. Kammerer, E. and Mourier, G., 1982, Development of gyrotrons at Thomson-CSF. Int. J. Electronics 53, 523.

Byerly, J.L., 1984, Harmonic emission from high power gyrotron oscillators. Masters Thesis, Department of Physics, Massachusetts Institute of Technology. (Unpublished).

Felch, K., Stone, D., Jory, H., Garcia, R., Wendell, G., Temkin, R.J., and Kreischer, K.E., 1982, Design and operation of magnetron injection guns for a 140 GHz gyrotron. Proc. Int. Electron Dev. Meeting.

Fliflet, A.W., and Read, M.E., 1981, Use of weakly irregular waveguide theory to calculate eigenfrequencies, Q valves, and RF field functions for gyrotron oscillators. Int. J. Electron. 51, 475.

Gaponov, A.V., Gol'denberg, A.L., Grigor'ev, D.P., Pankratova, T.B., Petelin, M.I., and Flyagin, V.A., 1975, Experimental investigation of centimeter-band gyrotrons. Radio Eng. and Electron. Phys. 18, 204.

Gilgenbach, R.M., Read, M.E., Hackett, K.E., Lucey, R., Hui, B., Granatstein, V.L., Chu, K.R., England, A.C., Loring, C.M., Eldridge, O.C., Howe, H.C., Kulchar, A.G., Lazarus, E., Marakami, M., and Wilgen, J.B., 1980, Heating at the electron cyclotron frequency in the ISX-B tokamak. Phys. Rev. Lett. 44, 647.

Guo He-Zong, Chen Zeng-Gui, Zhang Shi-Chang, and Wu De-shun, 1981, The study of TE_{02} mode gyromonotron operating at the second harmonic of the cyclotron frequency. Int. J. Electron. 51, 485.

Jory, H.R., 1977, Millimeter wave gyrotron development - phase 1. Technical Report RADC-TR-77-210, Contract No. F30602-76-C-0237.

Kreischer, K.E., and Temkin, R.J., 1983, High frequency gyrotrons and their application to tokamak plasma heating. Infrared and Millimeter Waves, vol. 7, K. Button, Ed., Academic Press, New York, p. 377.

Kreischer, K.E., Temkin, R.J., Fetterman, H.R., and Mulligan, W.J., 1984a, Multimode oscillation and mode competition in high frequency gyrotrons. IEEE Trans. microw. Theory Tech. 32, 481.

Kreischer, K.E., Schutkeker, J.B., Danly, B.G., Mulligan, W.J., and Temkin, R.J., 1984b. High Efficiency Operation of a 140 GHz pulsed

gyrotron. Int. J. of Electron. (elsewhere in this issue).

Kreischer, K.E., Danly, B.G., Woskoboinikow, P., Mulligan, W.J., and Temkin, R.J., 1984c, Frequency pulling and bandwidth measurements of a 140GHz pulsed gyrotron. Int. J. of Electron. (elsewhere in this issue).

Luchinin, A.G., Malygin, O.V., Nusinovich, G.S., and Flyagin, V.A., 1983, Submillimetier gyrotron with a pulsed magnetic field. Sov. Phys. Tech. Phys. 28, 1001.

Moiseev, M.A., and Nusinovich, G.S., 1974, Concerning the theory of multimode oscillation in a gyromonotron. Radiophys. Quantum Electron. 17, 1305.

Nusinovich, G.S., 1981, Mode interaction in gyrotrons. Int. J. Electron. 51, 457.

Nusinovich, G.S., and Erm, R.E., 1972, Efficiency of a CRM monotron with a longitudinal gaussian distribution of high frequency fields. Elektron. Tekh. Ser. 1, Elektron, SVCh No. 8, 55.

Silverstein, J.D., Curnutt, R.M., and Read, M.E., 1982, Near Millimeter wave radiation from a gyromonotron. Int. J. Electron. 53, 539.

Temkin, R.J., 1981, Analytic theory of a tapered gyrotron resonator. Int. J. Infrared and Millimeter Waves 2, 629.

Temkin, R.J., Kreischer, K.E., Mulligan, W.J., MacCabe, S., and Fetterman, H.R., 1982, A 100 kW, 140 GHz pulsed gyrotron. Int. J. Infrared and Millimeter Waves 3, 427.

Woskoboinikow, P., Cohn, D.R., and Temkin, R.J., 1983a, Application of advanced millimeter/far-infrared sources to collective Thomson scattering plasma diagnostics. Int. J. Infrared and Millimeter Waves 4, 205.

Woskoboinikow, P., Kreischer, K.E., Mulligan, W.J., and Temkin, R.J., 1983b, Bandwidth and frequency pulling of a 140 GHz gyrotron. Eighth Int. Conf. Infrared and Millimeter Waves Dig., IEEE Cat. No. 83CH1917-4.

Zapevalov, V.E., Zarnitsyna, I.G., and Nusinovich, G.S., 1979, Excitation of parasitic modes that resonate with the first harmonic of the cyclotron frequency in a gyrotron operating on a mode that resonates with the second harmonic. Radiophys. and Quantum Electron. 22, 254.

Zarnitsyna, I.G., and Nusinovich, G.S., 1977, Competition of modes resonant with different harmonics of cyclotron frequency in gyromonotrons. Radiophys. and Quantum Electron. 20, 313.

Zaytsev, N.E., Pankratova, T.B., Petelin, M.I., and Flyagin, V.A., 1974, Millimeter and submillimeter-wave gyrotrons. Radio Eng. and Electron. Phys. 19, 103.

Figure Captions

Figure 1. Starting current for $2\omega_c$ modes in 4-5T magnetic field range.

Figure 2. Starting current for $2\omega_c$ modes in 5-6T magnetic field range.

Figure 3. Diagram of Experimental Apparatus.

Figure 4. Diode scan showing both fundamental (unshaded) and second harmonic (shaded) zones of operation. The ordinate is a logarithmic scale.

Figure 5. Diode signals at magnetic field of 5.98T for second harmonic (top) and fundamental (bottom) modes. Horizontal time scale is 0.5μs/div.

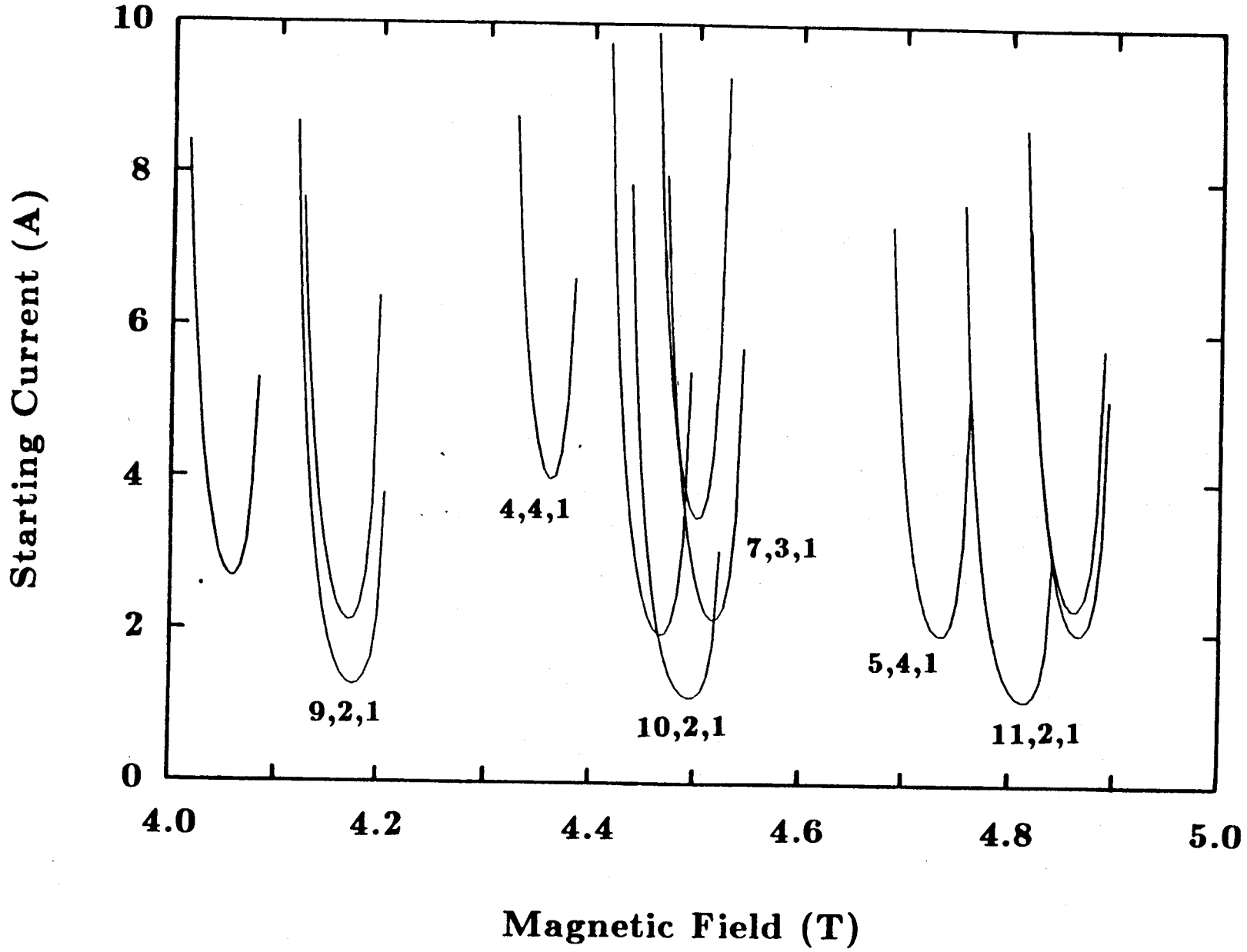
Starting Current (A)
10
8
6
4
2
0
4.0
4.2
4.4
4.6
4.8
5.0
Magnetic Field (T)
9,2,1
4,4,1
10,2,1
7,3,1
5,4,1
11,2,1

Fig. 1

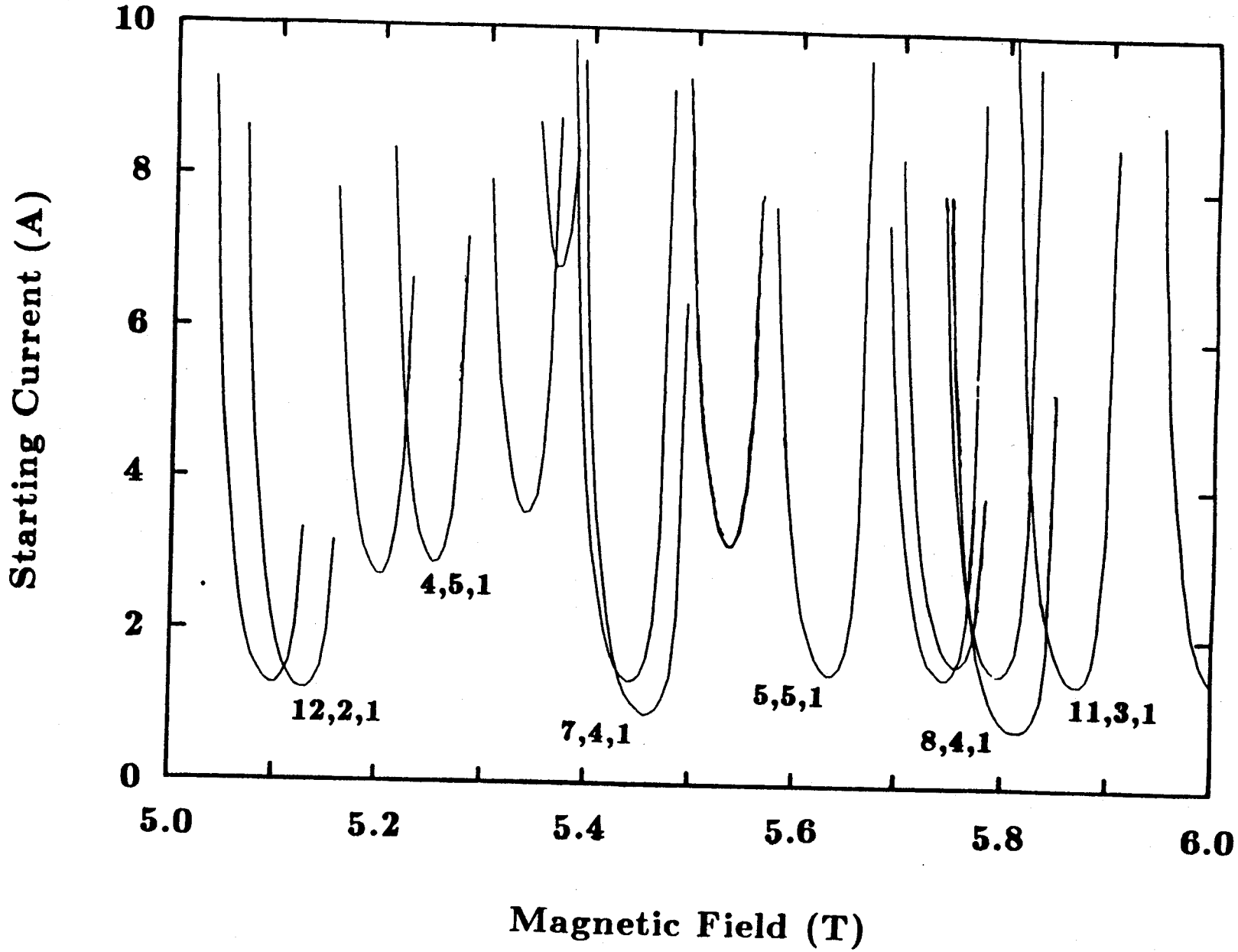
Starting Current (A)
10
8
6
4
2
0
5.0
5.2
5.4
5.6
5.8
6.0
Magnetic Field (T)
12,2,1
4,5,1
7,4,1
5,5,1
8,4,1
11,3,1

Fig. 2

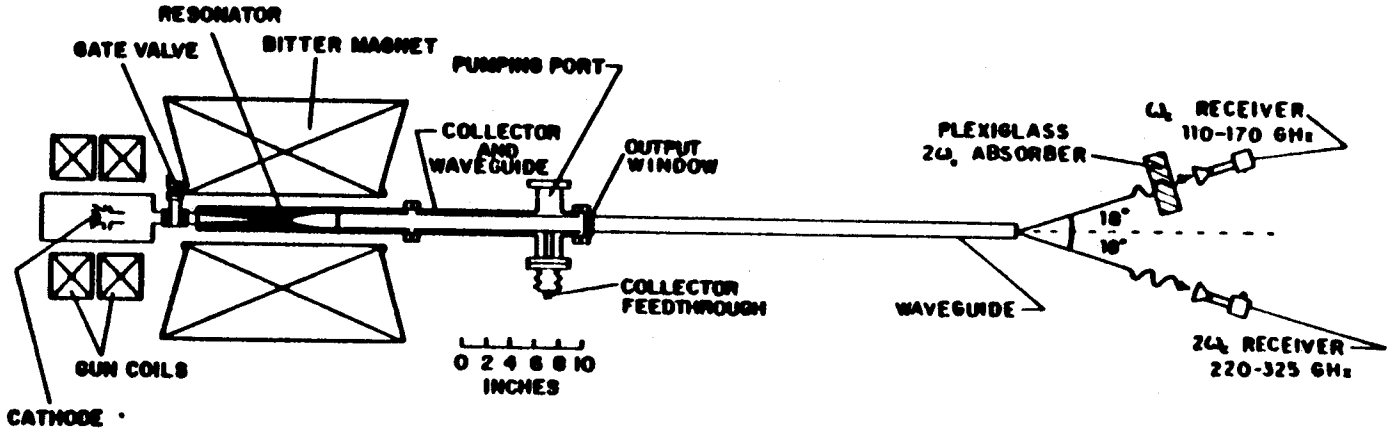
RESONATOR
GATE VALVE
BITTER MAGNET
PUMPING PORT
COLLECTOR AND WAVEGUIDE
OUTPUT WINDOW
PLEXIGLASS 2ω₀ ABSORBER
ω₀ RECEIVER 110-170 GHz
18°
18°
COLLECTOR FEEDTHROUGH
WAVEGUIDE
2ω₀ RECEIVER 220-325 GHz
GUN COILS
0 2 4 6 8 10
INCHES
CATHODE
M.I.T. 140 GHz GYROTRON

Fig. 3

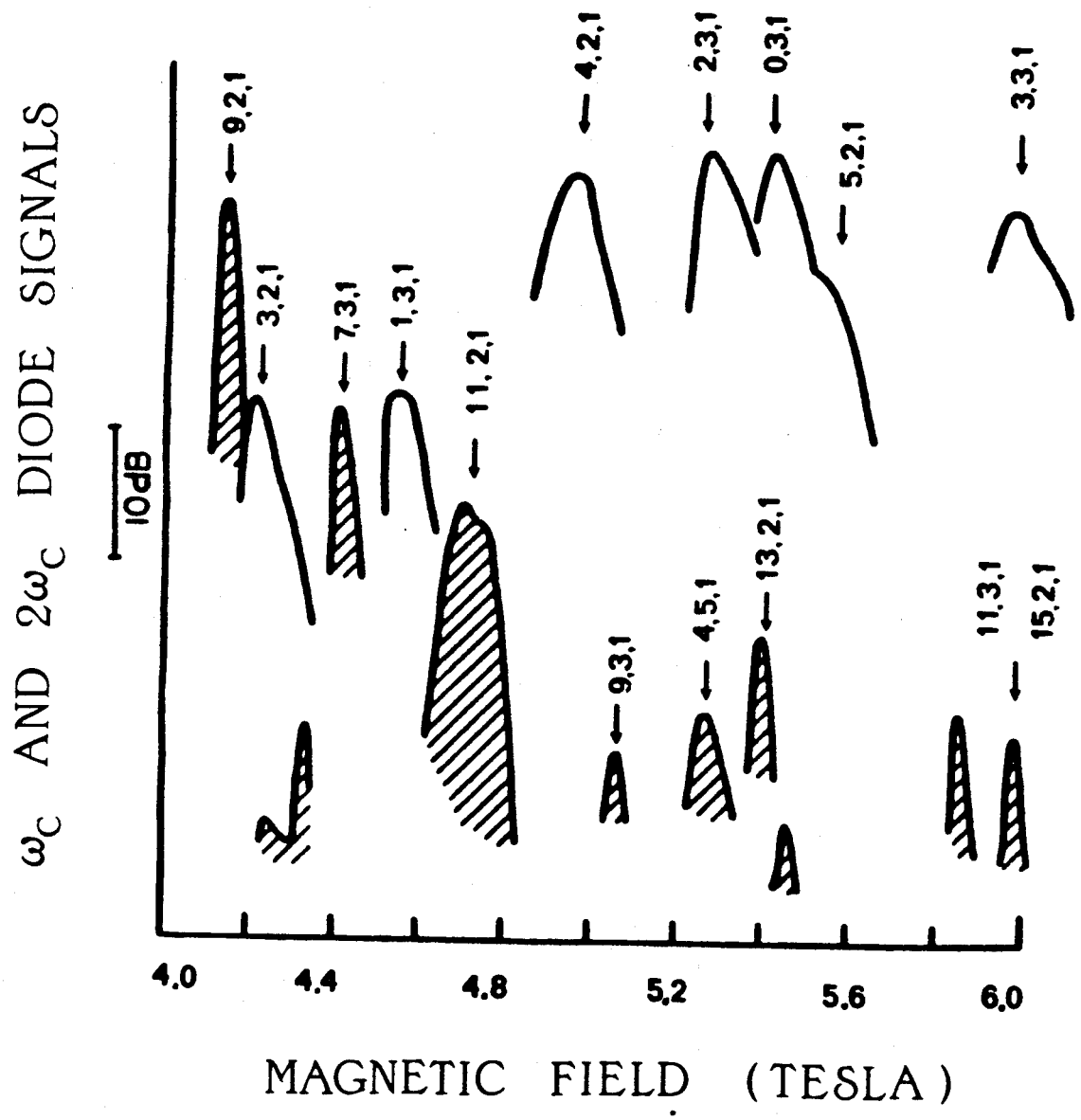
ωC AND 2ωC DIODE SIGNALS
10dB
9,2,1
3,2,1
7,3,1
1,3,1
11,2,1
4,2,1
2,3,1
0,3,1
5,2,1
3,3,1
9,3,1
4,5,1
13,2,1
11,3,1
15,2,1
4.0
4.4
4.8
5.2
5.6
6.0
MAGNETIC FIELD (TESLA)

Fig. 4

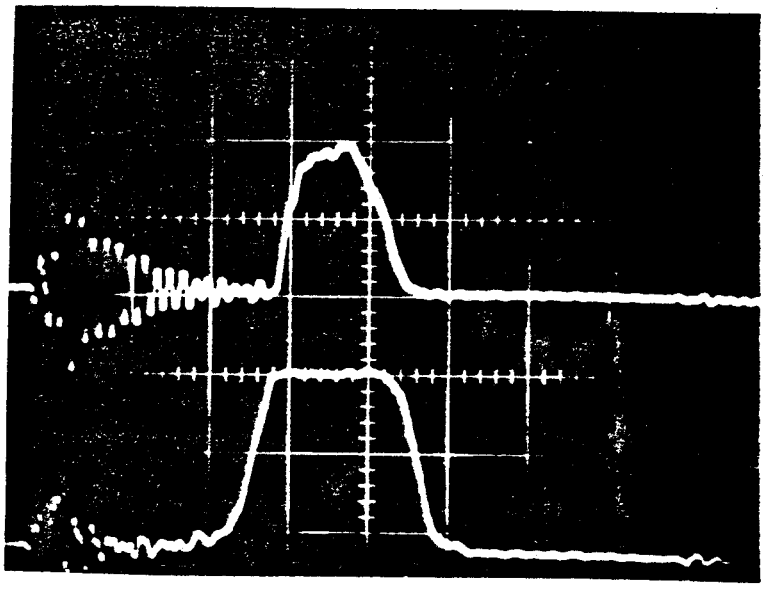

Fig. 5

Table 1 — $\omega \approx 2\omega_c$ Starting Currents

TE MODE	*CAVRF FREQUENCY (GHz)*	*MAGNETIC FIELD (T)*	I_{ST} *(A)*
1,5,1	203.72	4.06	2.72
13,1,1	204.61	4.08	56.7
6,3,1	209.26	4.17	2.15
9,2,1	209.51	4.18	1.30
4,4,1	218.78	4.36	4.05
14,1,1	218.94	4.37	86.1
2,5,1	224.03	4.47	2.00
10,2,1	225.40	4.50	1.16
0,5,1	225.71	4.50	3.55
7,3,1	226.52	4.52	2.19
15,1,1	233.24	4.65	134.
5,4,1	237.24	4.73	2.00
11,2,1	241.17	4.81	1.13
8,3,1	243.55	4.86	2.35
3,5,1	243.75	4.87	2.03
1,6,1	246.86	4.93	10.7
16,1,1	247.51	4.94	210.
6,4,1	255.37	5.10	1.31
12,2,1	256.84	5.13	1.25
9,3,1	260.39	5.20	2.74
17,1,1	261.76	5.23	354.
4,5,1	263.01	5.25	2.92
2,6,1	267.35	5.34	3.59
0,6,1	268.76	5.37	6.86
13,2,1	272.42	5.44	1.40
7,4,1	273.22	5.46	0.960
18,1,1	275.99	5.51	578.
10,3,1	277.07	5.54	3.19
5,5,1	281.89	5.63	1.51
3,6,1	287.33	5.74	1.47
14,2,1	287.92	5.75	1.65
1,7,1	289.95	5.80	1.52
19,1,1	290.20	5.80	957.
8,4,1	290.84	5.81	0.783
11,3,1	293.60	5.87	1.41
6,5,1	300.46	6.01	1.36
15,2,1	303.35	6.07	2.03

Table 2 — $\omega \approx 2\omega_c$ Efficiency Calculations

MODE	μ	I_o	Δ_{opt}	η (%)
1,5,1	15.79	1.3	0.31	20
6,3,1	16.13	1.6	0.33	22
9,2,1	16.15	2.5	0.37	26
4,4,1	16.72	0.81	0.18	14
2,5,1	17.04	1.6	0.32	22
10,2,1	17.13	2.5	0.37	25
0,5,1	17.15	0.90	0.19	14
7,3,1	17.19	1.4	0.30	20
5,4,1	17.85	1.5	0.31	21
11,2,1	18.10	2.4	0.35	23
8,3,1	18.24	1.2	0.30	18
3,5,1	18.25	1.4	0.30	21
6,4,1	18.97	2.2	0.34	24
12,2,1	19.06	2.1	0.33	21
9,3,1	19.28	0.99	0.18	15
4,5,1	19.44	0.96	0.25	14
2,6,1	19.71	0.77	0.24	13
0,6,1	19.80	0.40	0.15	9.9
13,2,1	20.02	1.7	0.31	19
7,4,1	20.07	2.8	0.35	25
10,3,1	20.31	0.79	0.20	16
5,5,1	20.60	1.7	0.29	21
3,6,1	20.94	1.8	0.29	21
14,2,1	20.98	1.3	0.23	16
1,7,1	21.10	1.7	0.29	20
8,4,1	21.16	3.2	0.35	25
11,3,1	21.32	1.7	0.29	19
6,5,1	21.66	1.8	0.31	21

Table 3 — Observed Second Harmonic Emission

TE MODE	*PREDICTED FREQUENCY (GHz)*	*MEASURED FREQUENCY (GHz)*	*MAGNETIC FIELD (tesla)*
9, 2, 1	209.51	209.43	4.13
7, 3, 1	226.52	226.39	4.40
11, 2, 1	241.17	241.02	4.70
9, 3, 1	260.39	260.29	5.09
4, 5, 1	263.01	263.31	5.26
13, 2, 1	272.42	272.24	5.39
11, 3, 1	293.60	294.08	5.98
15, 2, 1	303.35	302.40	5.98